Available online at www.sciencedirect.com
ScienceDirect
International Journal of Heat and Mass Transfer 51 (2008) 4985–5000
International Journal of HEAT and MASS TRANSFER
www.elsevier.com/locate/ijhmt

On the effects of Rayleigh number and inlet turbulence intensity upon the buoyancy-induced mass flow rate in sloping and convergent channels

B. Zamora, A.S. Kaiser *, A. Viedma

Dpto. Ingeniería Térmica y de Fluidos, Universidad Politécnica de Cartagena, Doctor Fleming s/n, 30202 Cartagena, Spain

Received 21 August 2006
Available online 28 April 2008

Abstract

A numerical study on the mass flow rate induced by natural convection in a sloped converging channel for different inclination and convergence angles with symmetrical heating is reported. Two-dimensional, laminar, transitional and turbulent simulations were obtained by solving the fully-elliptic governing equations using two different general purpose codes: Fluent and Phoenics. In transitional and turbulent cases, the low-Reynolds k–ω turbulence model was employed. Special emphasis was carried out, for turbulent regime, on the systematic comparisons of computational results with experimental and numerical data taken from literature, considering the influence of inlet turbulence intensity upon transitional point. Numerical results were obtained for wide and not yet covered ranges of the modified Rayleigh number varying from 10^{-2} to 10^{12}, the aspect ratio between 0.03 and 0.25, the converging angle from 1° to 30° and sloping angle from 0° to 60°. A generalized correlation for the non-dimensional mass flow rate in a channel with isothermal plates and symmetric heating conditions is presented.

Keywords: Convective flows; Sloped converging channels; Turbulence intensity

1. Introduction

Free convection phenomena plays an important role in design and performance of different problems, like naturally ventilated buildings or cooling of electronic components. For example, inducing higher mass flow rate results into obtaining better mixing in typical room ventilation applications. The geometries studied frequently involve structures based on converging and sloped channels formed by heated plates, where buoyancy-driven flows take place. So, the study of laminar and turbulent buoyancy-induced flows in these devices by a generalized geometry may be considered interesting from a fundamental point of view. As a consequence of the great scale of certain passive ventilation systems, as solar chimneys, Trombe walls or roof collectors, the flow established becomes transitional or even fully turbulent. In addition, important lacks over correlations for the buoyancy-induced mass flow rate have been detected. The main objective became for the present work to obtain a generalized correlation for the mass flow rate as a function of Rayleigh number, taking into account the effects of several geometrical parameters. This correlation could be employed in sizing methods of passive ventilation systems, for given conditions.

A large number of works published on laminar natural convection flow in channels exists; however, only few researches were reported on the turbulent case. Lloyd and Sparrow [1] analyzed the conditions of transition to turbulence for a flow induced by natural convection in an isolated vertical plate and they reported a value for the turbulence transition of Grashof number (based on the length of channel L) of 1.24×10^9. Miyamoto et al. [2] studied

* Corresponding author. Fax: +34 968 325 999.
E-mail address: antonio.kaiser@upct.es (A.S. Kaiser).

0017-9310/$ - see front matter © 2008 Elsevier Ltd. All rights reserved.
doi:10.1016/j.ijheatmasstransfer.2008.02.040

Nomenclature

b	minimum inter-plate spacing in the channel (Fig. 1)
c_p	specific heat at constant pressure
g	gravitational acceleration
Gr_l	Grashof number, $g\beta(T_w - T_\infty)l^3/\nu^2$ or $g\beta q l^4/\nu^2\kappa$
h_χ	local heat transfer coefficient, $\kappa(\partial T/\partial y)_w/(T_w - T_\infty)$
I	turbulence intensity, Eq. (15)
k	turbulent kinetic energy, Eq. (5)
L	streamwise length of wall (Fig. 1)
l	typical length, $l = L$ or $l = b$
$\dot{m}$	two-dimensional mass flow rate
n	coordinate perpendicular to wall
Nu_l	average Nusselt number, Eq. (18)
Nu_b, Nu_L	average Nusselt number based on b and L, respectively
$Nu_{l,\chi}$	local Nusselt number based on l
P	average reduced pressure
Pr	Prandtl number, ν/α
q	wall heat flux
Ra_l	Rayleigh number based on l, (Gr_l) (Pr)
Ra_x, Ra_χ	local Rayleigh number along the wall
Ra^*	modified Rayleigh number based on b, $Ra_b(b/L)$
Re	Reynolds number, Ul/ν
T, T'	average and turbulent temperature, respectively
T_w	wall temperature
T_∞	ambient temperature
$-T'u_j$	averaged turbulent heat flux
U	typical velocity
U_j, u_j	average and turbulent components of velocity, respectively
$-u_i u_j$	turbulent stress
u_τ	friction velocity $u_\tau = (\tau_w/\rho)^{1/2}$
x, y, z	cartesian coordinates (Fig. 1)
y^+	$\rho y u_\tau/\mu$, with y the distance between the wall and the first grid point

Greek symbols

α	thermal diffusivity, $\kappa/\rho c_p$
β	coefficient of thermal expansion, $1/T_\infty$
γ	converging angle (Fig. 1)
Θ	inclination angle (Fig. 1)
κ	thermal conductivity
μ, ν	viscosity and kinematic viscosity, μ/ρ, respectively
ρ	density
Φ	non-dimensional mass flow rate based on b, $\Phi = \dot{m}/\rho\nu Gr_b$
χ	coordinate along the wall (Fig. 1)
τ_w	wall shear stress
ω	specific dissipation rate of k (or turbulent frecuency)

Subscripts

bl	boundary layer limit
fd	fully developed limit
t	turbulent
w	wall
∞	ambient or reference conditions

experimentally turbulent flows in vertical channels formed by one of the plates with a constant heat flux and the other plate as adiabatic. They established the transition for a local Grashof number in the order of 10^{13}. Yan et al. [3] and Yan and Lin [4,5] analyzed different aspects of the laminar, transitional and turbulent regimes of the flow. Yuan et al. [6] proposed wall functions for numeric simulations of turbulent convective flows in vertical plates. Versteegh and Nieuwstadt [7] studied the scaling behaviour of natural convection flows between two infinite differentially heated vertical walls, to propose appropriate wall functions. Henkes and Hoogendorn [8] analyzed turbulent convection in enclosures.

Peng and Davison [9] employed the k–ω turbulence model to describe the convective turbulent flow within a cavity. Xu et al. [10] analyzed the flow established in a channel through a new model of turbulence which uses direct numerical simulation (DNS) in the region close to the wall and also they utilized the model k–ϵ for the region further away from the wall. Said et al. [11] studied the same problem for modified Rayleigh numbers (based on width of the channel, b) between 10^4 and 10^6, and sloping angles of the channel, between 0° and 90°, through a modified k–ϵ turbulence model.

Fedorov and Viskanta [12] employed the low-Re number k–ϵ turbulence model to calculate the induced flow and heat transfer in an asymmetrically heated, vertical parallel-plate channel. They compared their results with those obtained experimentally by Miyamoto et al. [13], and reported that the turbulence intensity at the channel inlet affects the location of transition from laminar to turbulent flow. Their results indicated that increasing turbulence intensity at the channel inlet causes the flow to be turbulent at downstream section.

Although a large number of studies on natural convection heat transfer in vertical channels have been reported, the induced mass flow rate has not deserve the same attention. Hajji and Worek [14] proposed an analytical solution to fully developed flow in a sloped channel. Lee [15] investigated analytically and experimentally the effects of considering unheated extensions at inlet or outlet of a vertical channel. Following works of Aung [16], Nelson and Wood [17] determined both heat transfer and air mass

flow within vertical channels with asymmetric heating conditions.

As it could be expected, the 'burnout' effects described by Guo and Wu [18] and Hernández and Zamora [19] can not appear in our computations, for the range of parameters and heating conditions studied. Hernández and Zamora [19] investigated the influence of variable property effects on laminar air flows in vertical channels under non-uniform heating and non-Boussinesq conditions. They carried out an analytical estimation of the critical wall heat flux, and they compared their results with those obtained by Guo and Wu [18].

In this way, most of the results reported were obtained for heat transfer parameters, while mass flow rate has deserved a minor attention mainly for turbulent regime. Indeed, this work is focused on the study of induced flow by natural convection in convergent and inclined channels (described in Fig. 1) in the laminar, laminar-turbulent transition and fully turbulent regimes with symmetrical isothermal heating, and aimed mainly on the induced mass flow rate through the channel.

The first part of the paper is focused on laminar flow. In the second one, the study of transitional and turbulent flow is broached, with special attention on the influence of turbulence intensity imposed at the inlet of the channel. Since our objective is to analyze the effects of Rayleigh number and initial turbulence intensity, principally over the induced mass flow rate, Boussinesq approximation and uniform properties for air are considered. Numerically, turbulent models as the standard k–ϵ, in combination with wall functions has been usually applied. Contrary to forced convection boundary layers, at the moment typical logarithmic wall functions seem to be not appropriate to calculate the natural convection boundary layer. In this way, the low-Reynolds k–ω turbulence model was employed to solve the cases considered in present research. The flow was assessed by using the Fluent and Phoenics codes, both based on a finite volume procedure. These codes were validated enough to solve natural convective flows. Successfully laminar results were obtained by authors in Kaiser et al. [20]. The working fluid is air, with a constant Prandtl number equal to 0.71. As it could be expected, the computational results obtained with Fluent and Phoenics are almost coincidental. However, some slight differences will be exposed.

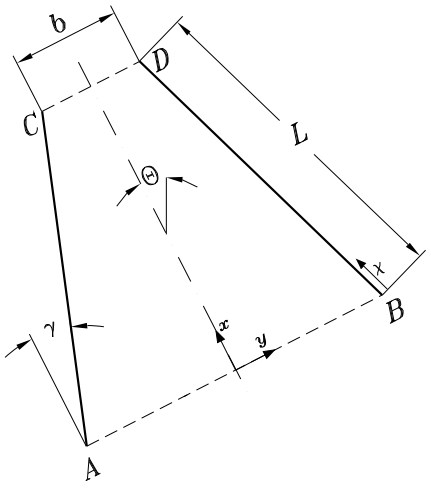

Fig. 1. Scheme of a converging sloped channel formed by isothermal AC and BD walls.

2. Mathematical model

2.1. Governing equations

Since the temperature variations are not too high, the Boussinesq approximation can be employed, assuming constants the thermophysical properties of the fluid, except for density variations in the buoyancy term in the vertical momentum equation. Applying this approximation, the simplified time-averaged Navier–Stokes equations of motion for steady, two-dimensional incompressible flow, can be written as follows:

$$\frac{\partial U_j}{\partial x_j} = 0, \tag{1}$$

$$\left(\frac{\partial U_i U_j}{\partial x_j}\right) = -\frac{1}{\rho}\frac{\partial P}{\partial x_i} - g_i\beta(T - T_\infty) + \frac{\partial}{\partial x_j}\left(\nu\frac{\partial U_i}{\partial x_j} - u_i u_j\right), \tag{2}$$

$$\frac{\partial (TU_j)}{\partial x_j} = \frac{\partial}{\partial x_j}\left(\frac{\nu}{Pr}\frac{\partial T}{\partial x_j} - T'u_j\right), \tag{3}$$

where U is the average velocity, T the average temperature, and P the average reduced pressure, difference between the pressure and the ambient pressure P_∞ (this given by the hydrostatic law, $\mathrm{d}P_\infty/\mathrm{d}x = -g\rho_\infty$); β is the thermal expansion coefficient (equal to $1/T_\infty$ for a perfect gas). The turbulent stress $-u_i u_j$ and turbulent heat flux $-T'u_j$ are supplied from the turbulence closure model, which are explained below, assuming that

$$-u_i u_j = 2\nu_t S_{ij} - \frac{2}{3}k\delta_{ij}, \quad \text{and} \quad -T'u_j = \frac{\nu_t}{Pr_t}\frac{\partial T}{\partial x_j}, \tag{4}$$

being ν_t and Pr_t the turbulent kinematic viscosity and turbulent Prandtl number, respectively; S_{ij} is the mean strain tensor, $S_{ij} = [(\partial U_i/\partial x_j) + (\partial U_j/\partial x_i)]/2$, δ_{ij} the Krönecker delta, and k the kinetic turbulent energy,

$$k = \frac{u_x^2 + u_y^2 + u_z^2}{2}. \tag{5}$$

Obviously, for fully laminar flow, $-u_i u_j = -T'u_j = 0$.

2.2. Turbulence model

The closure problem posed in Eqs. (1)–(3) is solved through the two transport equations low-Re k–ω model. This model has some advantages in transitional flows. No additional models were employed to lead the flow to transition at certain location in the flow field. The transition point takes place as a part of the solution of governing

transport equations. Moreover, it does not require the calculation of wall distances or damping functions based on the friction velocity. In this way, the k–ω model proposed by Wilcox [21] (from the model proposed originally by Kolmogorov [22]) has been used in the present study mainly because it allows the simulation of transitional flows. The model can be derived from the Navier–Stokes equations and it can written as follows:

– *Transport equation for kinetic turbulent energy* k,

$$U_j\frac{\partial k}{\partial x_j}=\frac{\partial}{\partial x_j}\left[\left(\nu+\frac{\nu_t}{\sigma_k}\right)\frac{\partial k}{\partial x_j}\right]+u_iu_j\frac{\partial U_i}{\partial x_j}-\beta^*f_{\beta^*}k\omega. \tag{6}$$

- In the diffusion term, the effective diffusivity is $\nu+(\nu_t/\sigma_k)$, and the kinematic eddy viscosity is given by

$$\nu_t=\alpha^*\frac{k}{\omega}, \tag{7}$$

being α^* a function that damps the turbulent viscosity causing a low-Re correction,

$$\alpha^*=\alpha^*_\infty\left(\frac{\alpha^*_0+Re_t/R_k}{1+Re_t/R_k}\right),\quad \text{with } Re_t=\frac{k}{\nu\omega}. \tag{8}$$

- The turbulence production term is $u_iu_j(\partial U_i/\partial x_j)$.
- In the turbulence dissipation term, $-(\beta^*f_{\beta^*}k\omega)$, the factor f_{β^*} is

$$f_{\beta^*}=\begin{cases}1, & \xi_k\leqslant 0\\ \frac{1+680\xi_k^2}{1+400\xi_k^2}, & \xi_k>0\end{cases},\quad \text{with } \xi_k\equiv\frac{1}{\omega^3}\frac{\partial k}{\partial x_j}\frac{\partial\omega}{\partial x_j}, \tag{9}$$

and β^* is a damping function of Re_t,

$$\beta^*=\beta^*_\infty\left(\frac{4/15+(Re_t/R_\beta)^4}{1+(Re_t/R_\beta)^4}\right). \tag{10}$$

The optative additional production of turbulent buoyancy, $-g_i\beta(\nu_t/Pr_t)(\partial T/\partial x_i)$, is neglected, since no stratification temperature fields is expected.

– *Transport equation for specific dissipation rate or turbulence frequency* ω (i.e., the ratio between the dissipation rate of k, and the same k),

$$U_j\frac{\partial\omega}{\partial x_j}=\frac{\partial}{\partial x_j}\left[\left(\nu+\frac{\nu_t}{\sigma_\omega}\right)\frac{\partial\omega}{\partial x_j}\right]+u_iu_j\frac{\partial U_i}{\partial x_j}\alpha\frac{\omega}{k}-\beta f_\beta\omega^2. \tag{11}$$

- In the production term, $u_iu_j(\partial U_i/\partial x_j)\alpha(\omega/k)$, α is another damping function,

$$\alpha=\frac{\alpha_\infty}{\alpha^*}\left(\frac{\alpha_0+Re_t/R_\omega}{1+Re_t/R_\omega}\right). \tag{12}$$

- In the dissipation term $-(\beta f_\beta\omega^2)$, f_β is

$$f_\beta=\frac{1+70\xi_\omega}{1+80\xi_\omega},\quad \text{with } \xi_\omega\equiv\left|\frac{\Omega_{ij}\Omega_{jk}S_{ki}}{(\beta^*_\infty\omega)^3}\right|, \tag{13}$$

being Ω_{ij} and S_{ki} the mean-rotation and mean-strain tensors, respectively, given by

$$\Omega_{ij}=\frac{1}{2}\left(\frac{\partial U_i}{\partial x_j}-\frac{\partial U_j}{\partial x_i}\right),\quad S_{ij}=\frac{1}{2}\left(\frac{\partial U_i}{\partial x_j}+\frac{\partial U_j}{\partial x_i}\right). \tag{14}$$

(ξ_ω is zero for two-dimensional flows, and so, $f_\beta=1$).

The following experimental constants complete the model: $R_k=6.0$, $\alpha^*_0=\beta_i/3$, $\alpha^*_\infty=1$, $\beta_i=0.072$, $R_\beta=8.0$, $\beta^*_\infty=0.09$, $\sigma_k=\sigma_\omega=2.0$, $R_\omega=2.95$, $\alpha_\infty=0.52$, $\alpha_0=1/9$, $\beta=\beta_i$. A constant value of $Pr_t=0.86$ for air is assumed in the computations.

2.3. Near-wall settings and boundary conditions

In transitional flows, the turbulence production does not have to balance itself with the turbulence dissipation close the walls, and the hypothesis of universality of the boundary layer profiles (the 'law of the wall', usually logarithmic) is not fulfilled. The k–ω model allows to use wall functions when mesh is sufficiently coarse near the wall, with $y^+>30$, or otherwise, to solve the flow within viscous sub-layer when the mesh becomes sufficiently fine and includes some nodes inside the viscous sub-layer, with non-dimensional sub-layer scaled distance $y^+\approx 1$.

At inlet section, the average reduced total-pressure imposed is $P_T=P+\rho(U_x^2+U_y^2)/2=0$. The air temperature is fixed equal to the ambient temperature T_∞. Since k- and ω-equations are homogenous, initial values of k and ω must be imposed to start computations. Indeed, the initial values for turbulent kinetic energy k is imposed by the way of a turbulence intensity,

$$I=\frac{[(2/3)k]^{1/2}}{U}, \tag{15}$$

where U is the main average velocity at the channel inlet. Thus, at inlet,

$$k_{inlet}=\frac{3}{2}I^2U^2,\quad \omega_{inlet}=\frac{k_{inlet}}{\nu_t}. \tag{16}$$

Turbulent intensity I is comprised between 2% and 30% in all the cases outlined. In order to obtain correlations for the induced mass flow rate, I is limited to 2%. Under certain conditions, conduction effects at inlet could be important. For laminar flows, Hernández et al. [23] studied the effect of including an entrance region to the domain. They reported that an extended computational domain at inlet is required only for cases with very low Rayleigh numbers. In this work, the diffusion effects at the channel inlet is neglected.

At outlet section, it is considered that the average reduced pressure is $P=0$. Since an initial value of velocity at inlet section is not known a priori in natural convection flows, a reference level for pressure is necessary for the elliptic numerical simulation of problem. Assuming that the flow discharges in a jet-like manner to the ambient at

exit, the streamwise variations of U_j, T, k and ω are neglected.

At walls, the no-slip boundary conditions is imposed on the average and turbulent velocity components. In isothermal cases, it is considered that $T = T_w$; at walls with a fixed heat flux q, it is imposed $\kappa(\partial T/\partial n) = q$, with n the coordinate perpendicular to wall, and at adiabatic walls, $\partial T/\partial n = 0$. For turbulent cases, $k = 0$ is imposed, and by means of a balance for the ω-equation, an asymptotic expression for ω as the wall is approached (see Wilcox [21]),

$$k = 0, \omega = \frac{Kv}{\beta^*_\infty y^2}, \tag{17}$$

being the theoretical value for K of 2. The value for ω given by Eq. (17) is employed to calculating ω at the computational first point adjacent to the wall surface.

3. Numerical computations

Results presented in this work were obtained by using both the general purpose Fluent and Phoenics codes, based on a finite volume procedure. In Fluent, the equations are discretised on a staggered-grid, using the 'Presto' scheme (similar to the staggered-grid scheme employed in Phoenics), with a second-order scheme for the convective terms. The Simple algorithm of Patankar and Spalding [24] was employed to solve the coupling between continuity and momentum equations through pressure. In Phoenics, the results were achieved employing a second-order differential scheme of 'Muscl' type for the convective terms [25]. The authors verified that using of alternative differential schemes produced nearly identical results. The convergence criterion in each case was $(\phi^{i+1} - \phi^i)/\phi^i \leqslant 10^{-5}$, where i denotes iteration number and ϕ can stand for any of the dependent variables.

In both Fluent and Phoenics codes, the turbulence model k–ω described previously was implemented. As a competitive advantage, the k–ω turbulence model revealed to be convergent enough in this work, for the wide range of Rayleigh number studied. The computations were carried out in a HPC160 (16 Alpha EV68CB−1 GHz) platform. For the majority of turbulent cases, CPU times around 25,000–30,000 s at least were necessary.

A structured, non-uniform mesh was built in both codes. The accuracy of the numerical results was tested by a grid dependence study. For laminar flow, a non-uniform grid of 120 cells in the x direction and 80 cells in the y direction was employed in most of cases. For both the horizontal and vertical direction, and for each grid and aspect ratio, power-law distribution was used to obtain a fine grid near-walls, as well as inlet and outlet sections. For transitional and turbulent flow, two parameters were considered to analyze the influence of the grid size: the y^+ and the number of cells in x and y directions. Fig. 2 shows the results obtained for a convergent channel with $Ra^* = 10^9$, aspect ratio $b/L = 0.1$, converging angle $\gamma = 12°$ and inclination angle $\Theta = 0°$, for y^+ varying between 0.09 and 123, and different grid sizes (64×48, 96×72, 120×80, 128×96, 176×132, 240×180, 280×210 and 400×300). For each grid size, the different values of y^+ were obtained by imposing different power-law distributions in y direction. For $y^+ \geqslant 2$, non-dimensional mass flow rate is affected mainly by the y^+ value and slightly by the number of cells, for each value of y^+. For values of y^+ lower than 2, this influence practically disappears and grid independence results are obtained. Following this study, the results presented were calculated using a non-uniform grid that gets y^+ lower than unity, including at least 10 grid points in the viscous sub-layer. Since ω values computed at the first grid node close to the wall were very high, strong relaxation factors for turbulent variables were employed to get enough accurate solutions.

4. Discussion of results

Numerical results have been obtained for modified Rayleigh number $10^{-2} \leqslant Ra^* \leqslant 10^{12}$, aspect ratio between $0.03 \leqslant b/L \leqslant 0.25$, converging angle $1 \leqslant \gamma \leqslant 30°$ and sloping angle $0 \leqslant \Theta \leqslant 60°$. First, laminar flow was broached. Second, transitional and turbulent flows were studied, with special attention on the influence of initial turbulence intensity.

Nusselt number has been calculated as follows:

$$Nu_L = \frac{1}{L}\int_0^L Nu_{l,\chi} \mathrm{d}\chi, \quad \text{with } Nu_{l,\chi} = h_\chi l/\kappa, \tag{18}$$

where h_χ is the local heat transfer coefficient, l a typical length and L the length of the channel.

The non-dimensional mass flow rate has been defined as

$$\Phi = \frac{\dot{m}}{\rho v Gr_b}, \tag{19}$$

with $\dot{m}$ is the two-dimensional mass flow rate, and Gr_b the Grashof number based on b.

4.1. First part: Laminar flow

Fig. 3 shows the results obtained for mass flow rate induced in a vertical channel ($\gamma = \Theta = 0$), for a wide range of modified Rayleigh number, $Ra^* = (Gr_b)(Pr)(b/L)$, and values of aspect ratio equal to $b/L = 0.03$ and 0.1. As expected, two different trends have been obtained: fully-developed (fd) regime for low enough Ra^*, and boundary layer (bl) regime, for high enough Ra^*. There is an excellent agreement between numerical results and the asymptotical solution given by Hajji and Worek [14]:

$$\Phi_{\mathrm{fd}} = \Phi_\infty \left[1 - \left(\frac{1}{24}\right)\Phi_\infty Ra^*/Pr\right], \tag{20}$$

with Φ_∞ the value of Φ_{fd} when $b/L \to 0$, equal to 1/12. For values of Ra^* between 10^{-2} and 1, deviation of

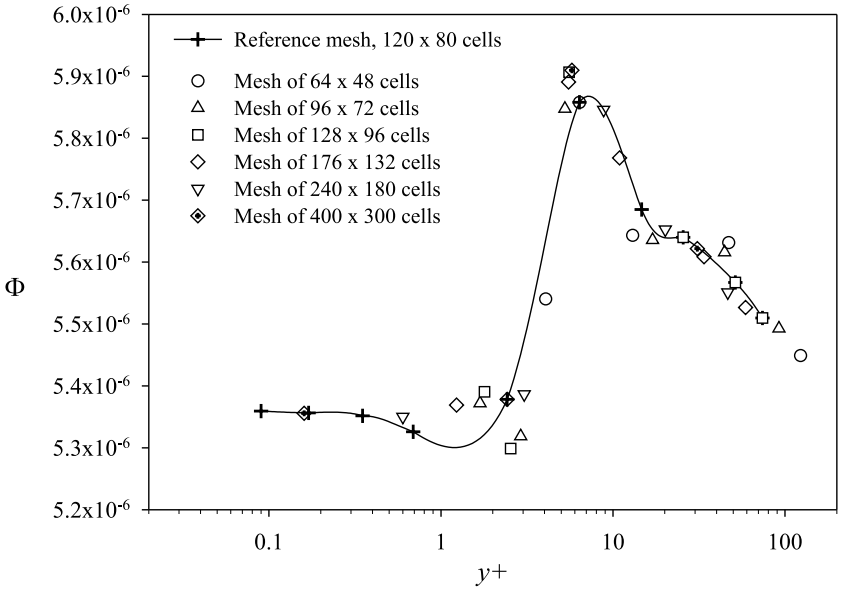

Fig. 2. Influence of number of cells and y^+ values on numerical results. $Ra^* = 10^9$, $b/L = 0.1$, $\gamma = 12°$, $\Theta = 0°$.

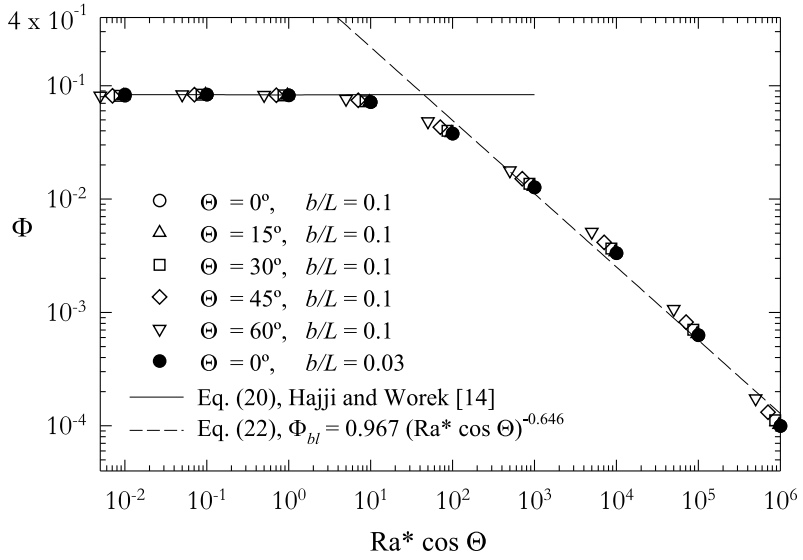

Fig. 3. Non-dimensional mass flow rate Φ as a function of modified Rayleigh number Ra^* and sloping angle Θ, for a channel with isothermal heating, converging angle $\gamma = 0°$, and aspect ratios $b/L = 0.03$ and 0.1.

numerical results with regards to above expression was of 1%. In boundary layer regime, although dimensional mass flow rate $\dot{m}$ increases as Ra^* increases, that augmentation is lower than the increasing of buoyancy forces (i.e., Grashof number). Then, dimensionless mass flow rate Φ decreases when Ra^* increases, as it could be appreciated in Fig. 3. The results obtained were fitted to following expression:

$$\Phi_{\mathrm{bl}} = \mathscr{A}(Ra^*)^{\mathscr{B}}, \tag{21}$$

with $\mathscr{A} = 0.967$ and $\mathscr{B} = -0.646$. For $10^3 \leqslant Ra^* \leqslant 10^5$, deviation was about 7 %. Taking into account the non-dimensional parameters defined above, results obtained were almost independent on channel aspect ratio b/L.

4.1.1. Influence of sloping angle

For the cases studied in this research, the influence of sloping angle regards to vertical axis, Θ, is taken into account including the factor $(\cos\Theta)$ in the definition of the Rayleigh number. Said et al. [11] have proposed the factor $(\cos\Theta)^{0.5}$. The utilization of Rayleigh number based on $(\cos\Theta)$ factor means the assumption of a widely employed practice for inclined plates. In a converging or sloping channel, the buoyancy force is no longer solely in the streamwise direction, since a component also exists perpendicular to the heated wall. Thus, the specific buoyancy force that accelerates the fluid in the thermal boundary layer is $[g\beta(T_w - T_\infty)\cos\Theta]$ instead of $[g\beta(T_w - T_\infty)]$. Later on, a correlation for the case of fully turbulent flow,

which includes both the sloping angle (Θ) and the convergence angle of the plates (γ), will be exposed. The specific buoyancy force is $[g\beta(T_w - T_\infty)\cos\Theta\cos\gamma]$ in the last case.

Cases made with $\Theta = 15°$, 30°, 45° and 60°, and aspect ratio $b/L = 0.03$ and 0.1 were computed. Results are compared with those obtained by Hajji and Worek [14] for dimensionless mass flow rate, and a good agreement is found, as shows Fig. 3, where Ra^* is modified through $(\cos\Theta)$. Once again, the influence of b/L results almost negligible. In a similar way that above, the boundary layer correlation for Φ can be written as:

$$\Phi_{bl} = \mathscr{A}(Ra^*\cos\Theta)^{\mathscr{B}}, \tag{22}$$

fitting also with $\mathscr{A} = 0.967$ and $\mathscr{B} = -0.646$, for $10^3 \leqslant Ra^* \leqslant 10^5$ and a deviation about 7%.

4.1.2. Influence of converging angle

For converging and sloping channels, best correlation of results obtained was reached by using the minimum inter-plate spacing [20]. It can be observed in Fig. 4 that numerical results do not follow the same asymptotical fully-developed behaviour at low enough Ra^* for different values of γ. For converging channel, with dimensionless governing parameters based on minimum inter-plate spacing, $\dot{m}$ increases as well as converging angles does, for a low enough Ra^*. The reason for that might be the augmentation of fluid volume under buoyancy force. In a previous work, Kaiser et al. [20], an asymptotic correlation for average Nusselt number and for fully-developed regime was obtained by the assumption of differential body forces over the flow field. As reported in that previous work, the relative increase of specific buoyancy force with respect to a vertical parallel channel of $b \times L$ dimensions was proportional to $(\cos\gamma)(\sin\gamma)$. Taking this into account, next expression

$$\Phi_{fd} = \Phi_\infty\left[1 + 3.0\frac{(\cos\gamma)^2(\sin\gamma)}{\Phi_\infty}\right], \tag{23}$$

adjust accurately to numerical results, for low enough Ra^*, with $\Phi_\infty = 1/12$.

The boundary layer expression for dimensionless mass flow rate takes the form:

$$\Phi_{bl} = \mathscr{A}(Ra^*\cos\gamma)^{\mathscr{B}}, \tag{24}$$

fitting with $\mathscr{A} = 0.967$ and $\mathscr{B} = -0.646$, as expected, for $10^3 \leqslant Ra^* \leqslant 10^5$ and also a deviation about 7%.

4.1.3. Influence of slope and converging angles

To find the combined influence of both sloping and converging angles, additional computations for $\Theta = 15°$, 30°, 45° and 60°, for $\gamma = 15°$ and $\gamma = 30°$ were carried out. The overlapping of results obtained (see Fig. 5, for $\gamma = 30°$ and $b/L = 0.1$) takes place by changing Ra^* by $Ra^*(\cos\Theta)(\cos\gamma)$. In this way, for boundary layer regime $(10^3 \leqslant Ra^* \leqslant 10^5)$,

$$\Phi_{bl} = \mathscr{A}(Ra^*\cos\Theta\cos\gamma)^{\mathscr{B}}, \tag{25}$$

closed obviously with $\mathscr{A} = 0.967$ and $\mathscr{B} = -0.646$, as the cases corresponding to $\gamma = \Theta = 0°$. In order to simplify, the slight influence of b/L on coefficients $\mathscr{A}$ and $\mathscr{B}$ is neglected. The effects of b/L will be retained on the blended-correlation exponent n, described later.

4.1.4. Generalized correlation proposed

According to numerical results presented in this paper for laminar flow, a correlation is determined both for fully-developed and for boundary layer regimes, by using the general expression suggested by Churchill and Usagi [26],

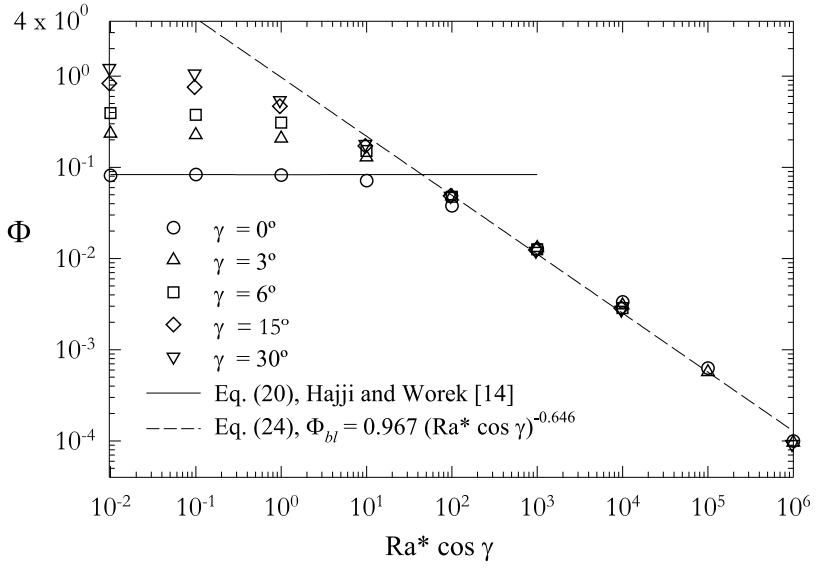

Fig. 4. Non-dimensional mass flow rate Φ as a function of modified Rayleigh number Ra^* and converging angle γ, for a channel with isothermal heating, sloping angle $\Theta = 0°$, and aspect ratio $b/L = 0.1$.

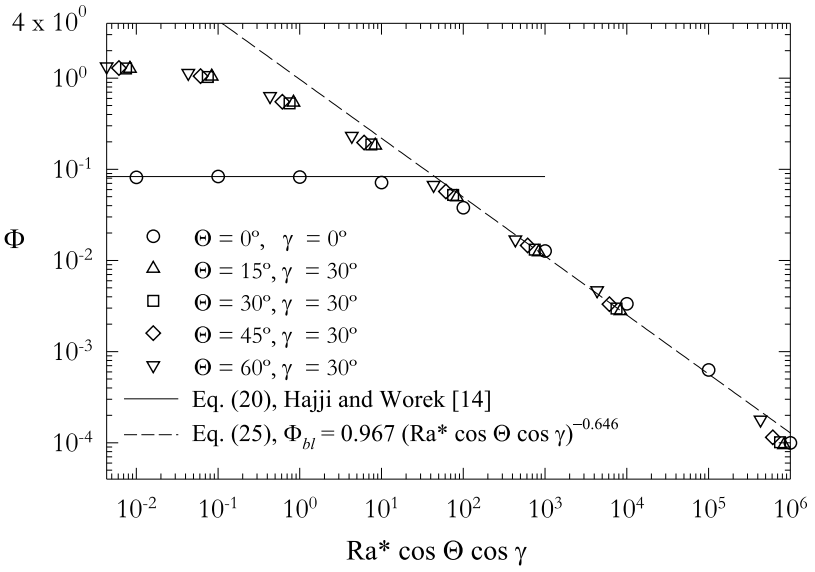

Fig. 5. Non-dimensional mass flow rate Φ as a function of $Ra^*(\cos\Theta)(\cos\gamma)$, for a channel with isothermal heating, $\gamma = 30°$, $\Theta = 15°, 30°, 45°, 60°$, and aspect ratio $b/L = 0.1$. Comparison with the case corresponding to $\gamma = \Theta = 0$.

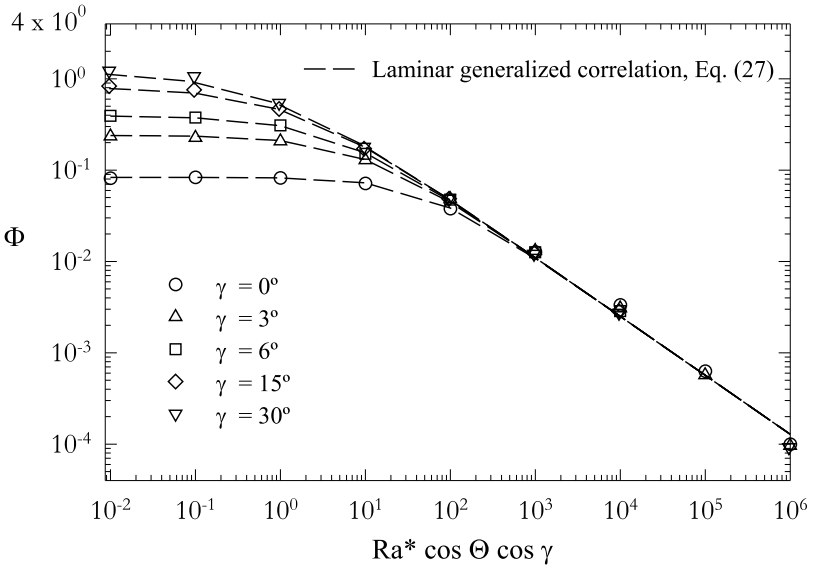

Fig. 6. Global correlation for non-dimensional mass flow rate as a function of $Ra^*(\cos\Theta)(\cos\gamma)$ and converging angle γ, for a channel with isothermal heating, $\Theta = 0°$ and $b/L = 0.1$.

$$\Phi = [\Phi_{\mathrm{fd}}^n + \Phi_b^n]^{1/n}, \tag{26}$$

where n is a blended coefficient. The global correlation takes the form (see Fig. 6):

$$\Phi = \left\{ \left[\Phi_\infty \left(1 + 3.0 \frac{(\cos\gamma)^2 (\sin\gamma)}{\Phi_\infty} \right) \right]^n + \left[0.967 (Ra^* \cos\Theta \cos\gamma)^{-0.646} \right]^n \right\}^{1/n}. \tag{27}$$

The value of n is obtained by correlating the numerical results obtained in this work. This exponent, as a function of b/L and γ, may be determined by:

$$n = -\frac{1}{6} \left(9.0 - \frac{\sin^{1/3}\gamma}{0.14 + (b/L)} \right). \tag{28}$$

Correlation (27) fits to numerical results for $Ra^* = 10^{-2}$ to 10^5, $0 \leqslant \Theta \leqslant 60°$, $0 \leqslant \gamma \leqslant 30°$, and $b/L = 0.03$ to 0.25, with an average error about 6%.

4.2. Second part: Turbulent flow

Fig. 7 shows a comparison between results obtained in this work and those reported by using the k–ϵ turbulence model by Akbari and Borgers [27] and Chen [28], for asymmetrical heating conditions. Although the results presented show a similar trend, some difference can be observed,

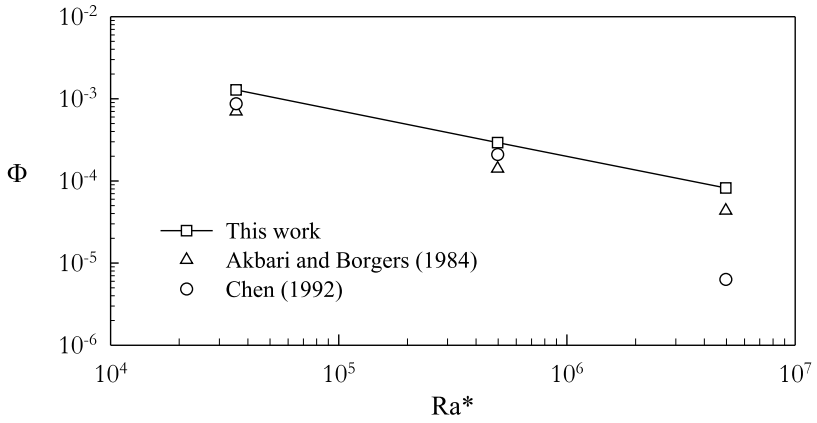

Fig. 7. Comparison of non-dimensional mass flow rate obtained by Akbari and Borgers [27] and Chen [28], and those obtained in this work, for a channel with asymmetric heating conditions and turbulent flow. $\gamma = \Theta = 0^\circ$.

mainly with respect to the results presented by Chen [28], for high Ra^*. These differences may be due to the fact that Chen [28] analyzed a different configuration, including specific horizontal inlet and outlet regions.

Versteegh and Nieuwstadt [7] studied, through DNS, the flow induced by natural convection in a vertical channel with a temperature difference between isothermal walls of 39.1 °C, enough to reach the turbulent regime with the geometrical and physical conditions considered. They avoid resolving the transition from laminar to turbulent regime. Aiming to validate their numeric results, these authors present experimental results of some of the analyzed cases. Fig. 8 shows the profiles of non-dimensional velocity obtained with DNS and experimentally by Versteegh and Nieuwstadt [7], and also the profiles obtained in this work by means Fluent and Phoenics codes. It can be observed a good agreement between our results and those obtained experimentally. In addition, although results are not shown, a good agreement between our results and those obtained by Habib et al. [29] was also reached.

In high turbulent flows induced by natural convection in channels, thermal boundary layers close to both walls are very thin and they practically do not interfere one to each other. The core region remains mainly unheated, and the heat transfer rate do not depend on inter-plate spacing. Described behaviour is not reproduced for mass flow rate, probably due to the larger velocity gradients reached in turbulent boundary layers, which carry away, near enough to these shear-wall layers, an appreciable amount of fluid, arising out of the core region. This reveals a relevant influence of viscosity even into regions relatively detached from walls. So, since mass flow rate has been obtained by across integration of velocity profile, aspect ratio appears as an outstanding parameter.

The following considerations about the form of correlations can be made. In literature, correlations for average

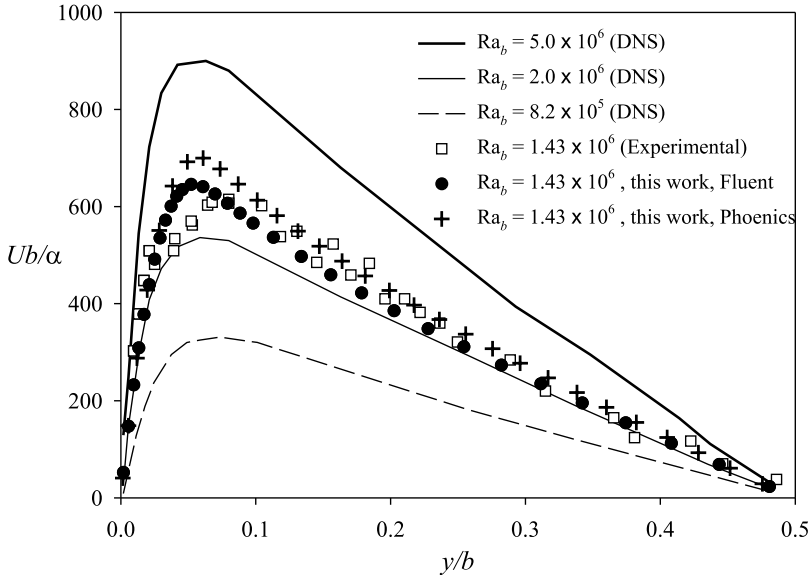

Fig. 8. Comparison between velocity profiles obtained in this work (using Fluent and Phoenics codes) with those obtained by Versteegh and Nieuwstadt [7], for a vertical channel with isothermal heating. $\gamma = \Theta = 0^\circ$. $b/L = 1/28.6$ and $b = 0.076$ mm.

Nusselt number (based on b) were reported usually as a function of Ra^*, for laminar flow. For turbulent cases, as widely employed practice, the thermic behaviour of flow was assimilated to that corresponding to an isolated plate, i.e., assuming that influence of inter-place spacing of the channel is negligible. Since thermal boundary layer is very thin for fully turbulent flow, best correlation of average Nusselt number (based on L) might be based on Ra_L. As aforementioned, in this work, a different behaviour of turbulent velocity boundary layer, was observed. Thus, it can be expected the next correlation form for the mass flow rate $\Phi \sim \mathscr{A}(Ra^*(b/L)^{\mathscr{C}})^{\mathscr{B}}$.

The results obtained for Φ in vertical channels varying Ra^* from 10^4 to 10^{12} have been reported in Fig. 9, for values of aspect ratio from 0.03 to 0.25. It can be observed that results obtained using both Fluent and Phoenics codes follow a same trend. The following correlation fits to numerical results obtained with Fluent:

$$\Phi = \mathscr{A}\left(Ra^*(b/L)^{\mathscr{C}}\right)^{\mathscr{B}}, \tag{29}$$

with $\mathscr{A} = 0.2$, $\mathscr{B} = -0.544$ and $\mathscr{C} = 0.54$. For $10^7 \leqslant Ra^* \leqslant 10^{12}$, average deviation between numerical results and above expression is equal to 7%.

4.2.1. Influence of sloping angle

In the results obtained through this research, it can be observed that as the sloping angle of the centreline of the

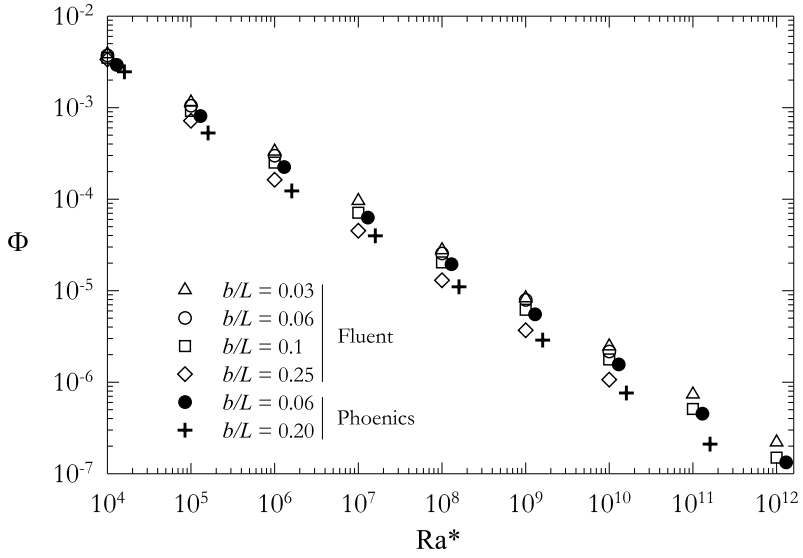

Fig. 9. Non-dimensional mass flow rate as a function of Ra^* for different values of b/L. Isothermal channel with symmetrical heating. $\gamma = \Theta = 0°$.

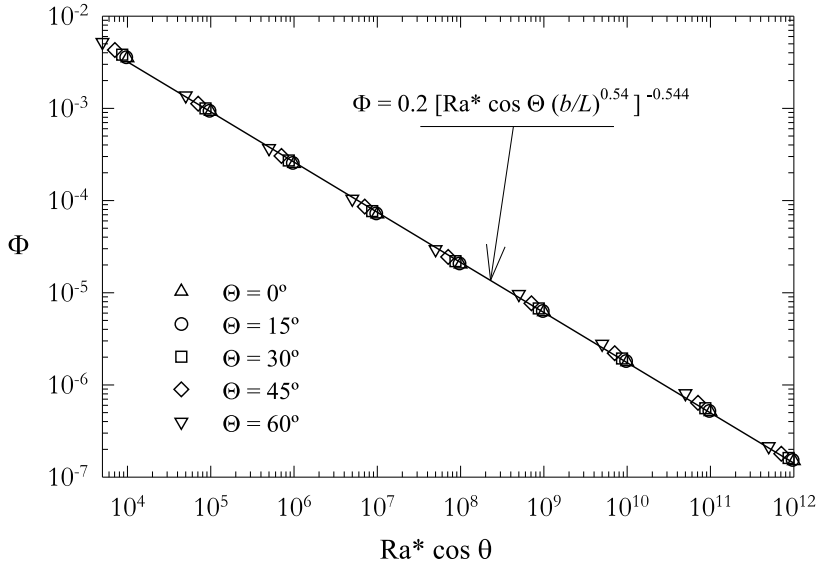

Fig. 10. Influence of sloping angle over non-dimensional mass flow rate in an inclined channel. Isothermal, symmetrical heating conditions. Numerical correlation proposed. $\gamma = 0°$, $b/L = 0.1$.

channel increases, the difference between the turbulence intensity generated in the lower plate with respect to that generated in the upper one, increases too. It can also be appreciated an asymmetrical field of velocity in the channel exit. Results obtained fit an expression like (29), including $(Ra^* \cos \Theta)$ instead of Ra^*. This can be observed in Fig. 10.

4.2.2. Influence of converging angle

Fig. 11 shows results obtained for Φ as a function of Ra^* and γ. It can be appreciated a change of trend in the results of Φ for a Ra^* of the order of 10^5, for $b/L = 0.1$ and $\Theta = 0^\circ$, agreeing with the statements by Churchill and Chu [30], which summarise the transition from laminar to turbulent regime for vertical plates in $Ra_L \approx 10^9$ (note that for $Ra^* = 10^5$ and $b/L = 0.1$, $Ra_L = Ra^* \times (b/L)^4 = 10^9$). Then, according with above papers analyzed, the roughly limit $Ra_L = 10^9$ can be accepted as good for transitional point from laminar to turbulent flow, for isolated plate and for channels with high aspect ratio, taking into account some light deviations caused by geometrical parameters (as sloping angles). The influence of the initial turbulence intensity considered will be exposed later. Results obtained fit an expression like (29), including $(Ra^* \cos \gamma)$ instead of Ra^* (see Fig. 11).

4.2.3. Influence of slope and converging angles. Generalized correlation

In order to obtain the influence of the sloping angle on Φ in convergent channels for turbulent regime, the cases presented were solved for converging angles of $\gamma = 15^\circ$ and

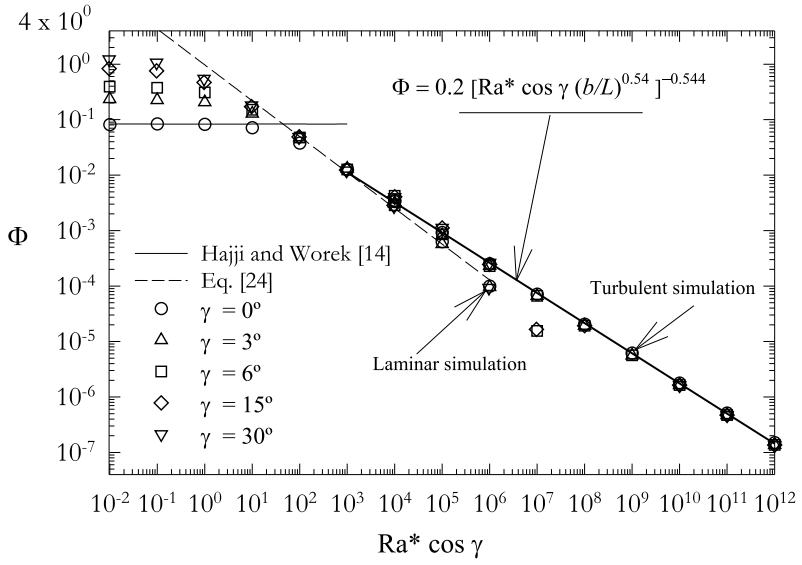

Fig. 11. Influence of converging angle over non-dimensional mass flow rate, as a function of Ra^*. Isothermal, symmetrical heating conditions. $\Theta = 0^\circ$, $b/L = 0.1$. Numerical correlation proposed.

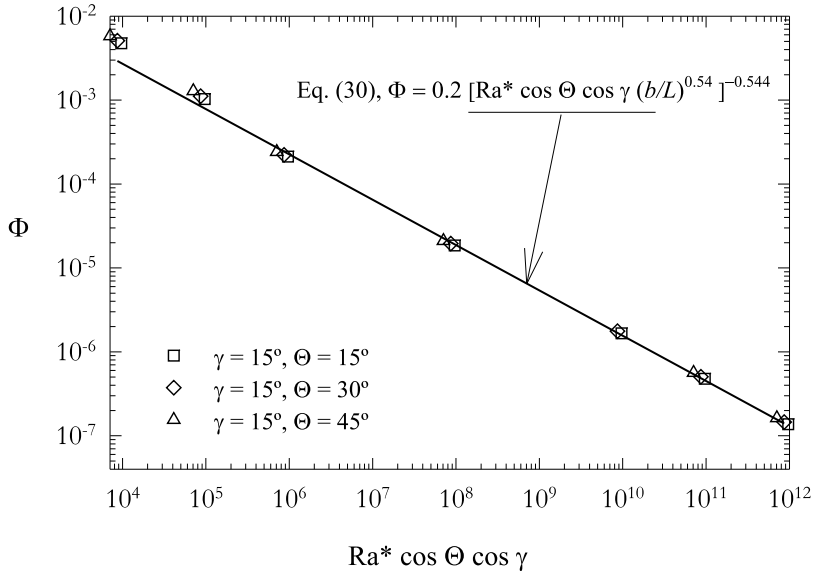

Fig. 12. Overlapping of results obtained for non-dimensional mass flow rate, for turbulent flow. Isothermal, symmetric heating conditions. Numerical correlation proposed.

30°, and for sloping angles of the channel $\Theta = 15°$, 30°, 45° and 60°. Once again, the factor $(\cos\Theta\cos\gamma)$ leads to obtain the overlapping of results (see Fig. 12).

The results obtained for Φ, in turbulent regime, within of a channel with symmetrical heating, including the effects of aspect ratio, sloping and convergence angles, can be collated by the following correlation (see Fig. 12):

$$\Phi = \mathscr{A}[Ra^*\cos\Theta\cos\gamma(b/L)^{\mathscr{C}}]^{\mathscr{B}}, \tag{30}$$

also with $\mathscr{A} = 0.2$, $\mathscr{B} = -0.544$ and $\mathscr{C} = 0.54$, for $10^7 \leqslant Ra^* \leqslant 10^{12}$, $0° \leqslant \gamma \leqslant 30°$, $0° \leqslant \Theta \leqslant 60°$, and for the wide range of values of b/L studied. The average error was equal to 6.4%. Note that rearranging Eqs. (25) and (30) as a function of Rayleigh number based on L, leads to $\Phi \sim Ra_L^{-0.646}(b/L)^{-2.584}$, and $\Phi \sim Ra_L^{-0.544}(b/L)^{-2.470}$, for laminar boundary layer regime, and fully-developed turbulent flow, respectively. While dependence on Rayleigh number changes significantly (19%), the exponents obtained for b/L are similar (a discrepancy of 4.6%), so, the influence of aspect ratio on the non-dimensional mass flow rate is mainly the same, for both boundary layer laminar and fully turbulent regimes.

4.2.4. Influence of turbulence intensity

4.2.4.1. Validation of the numerical results. In Fig. 13, numerical results are compared with those obtained experimentally by Miyamoto et al. [13], for a channel of $L = 5$ m, $b = 95$ mm, with asymmetrical heating. One plate remained adiabatic, while in the other one a heat flux equal to 208 W/m^2 was imposed (this case corresponds to $Ra_L = 5\times10^{14}$). For a low value of turbulence intensity, $I = 2\%$, a change of trend in results obtained for local Nusselt number Nu_x seems to indicate the transition to turbulent flow at a section next to the channel outlet. Experimental results show that transition occurs at a preceding section. It is possible to fit numerical results to experimental results by means of adjusting the turbulence intensity. Indeed, best agreement with regards to experimental data is reached for $I = 2.5\%$. For higher values of I ($I = 5\%$, 10%), the flow becomes fully turbulent, and numerical results obtained are greater than those obtained by Miyamoto et al. [13].

Fedorov and Viskanta [12] showed the strong influence exerted by the turbulence intensity I in the local heat transfer at the inlet of the channel. They presented distributions of Nu_x along the wall of an isothermal channel with asymmetrical heating, for $Gr_b = 2\times10^5$, 4×10^5, 6×10^5 and 10^6, and $I = 0$, 10 and 30%. Their results shown that for $Gr_b = 4\times10^5$ and $I = 0$, the flow evolved from laminar to turbulent at $x/L = 0.84$. As the Grashof number increased further, the transitional point moved closer to the inlet; for $Gr_b = 10^6$, the transition took place at $x/L = 0.64$. An increase in I at the inlet of channel yielded an advance in transition. At the moment, results obtained in present work have reproduced the same behaviour. However, since above cases of Fedorov and Viskanta [12] have been simulated in this work, some difference has been detected. In Fig. 14, it can be observed that laminar flow remains for $Gr_b = 2$, 4 and 6×10^5, transition occurs for $Gr_b = 10^6$, and higher values of I yield a strong turbulent flow for the same value of $Gr_b = 10^6$. For $I = 30\%$, average Nusselt number is a 31% higher than corresponding value to $I = 0$, for $Gr_b = 10^6$.

With regards to the influence of γ and Θ, additional computations were carried out for $\gamma = 6°$ and 15°, and $\Theta = 30°$. It can be observed in the added graph of Fig. 14 that increases of γ and Θ drive to obtain lightly higher Nusselt numbers, for the transitional value of Ra_L

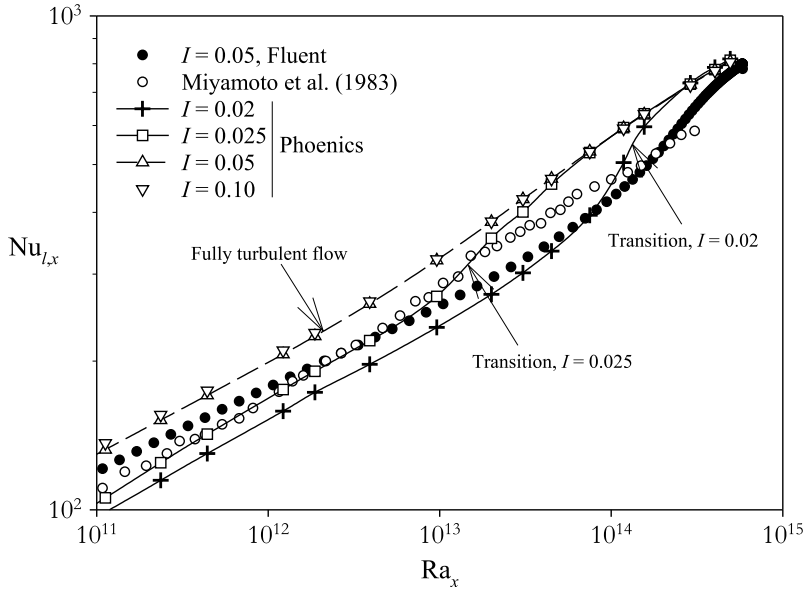

Fig. 13. Comparison with experimental results reported by Miyamoto et al. [2], for an isothermal asymmetrically heated channel, imposing a heat flux at one of walls equal to 208 W/m^2, and $b = 95$ mm, $L = 5$ m, $Ra_L = 5\times10^{14}$. $\gamma = \Theta = 0°$.

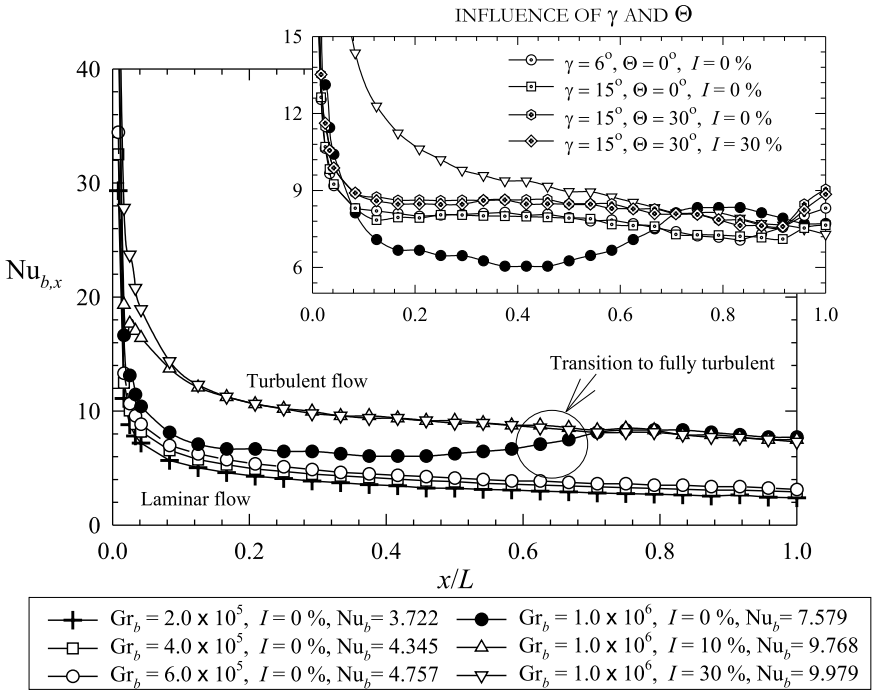

Fig. 14. Distribution of local Nusselt number along heated wall for a channel with asymmetrical heating (one plate isothermal, one plate adiabatic), for different values of Gr_b and turbulence intensity I. $b/L = 0.0125$.

outlined. However, the influence of I seems to be negligible as well as γ and Θ increases. This effect will be explained in the following section.

4.2.4.2. Effects of I on the thermal behaviour. An important aspect on design considerations is to fixe the suitable turbulent excitation so as to obtain transition to turbulence; however, a meaningful physical flow must be maintained. In thermal passive systems, no external mechanical devices are employed. A low value of initial turbulence at inlet must be considered, since it is not expected additional turbulence generating. In order to study the influence of I in a more systematic way, results for Nu_L were obtained in a vertical channel ($\gamma = \Theta = 0$), for turbulence intensity

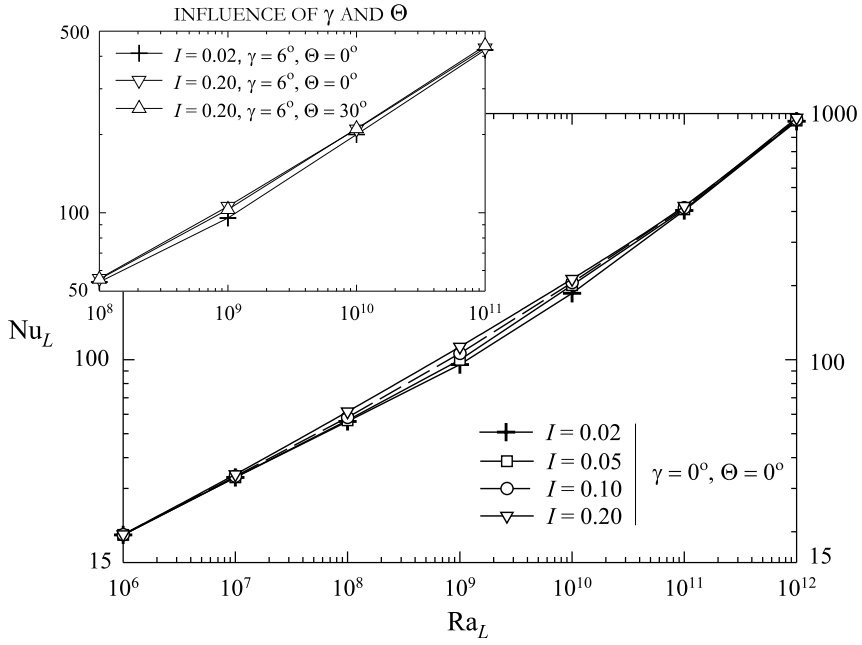

Fig. 15. Average Nusselt number Nu_L as a function of Ra_L. Influence of turbulence intensity I on the transitional range of Ra_L. Isothermal, symmetric heating conditions. $b/L = 0.2$.

$I = 0.02$, 0.05, 0.1 and 0.2, a range of Rayleigh number $10^6 \leqslant Ra_L < 10^{16}$, $b/L = 0.2$, and isothermal symmetric heating. Additional computations with $\gamma = 6^\circ$ and 15°, and $\Theta = 30^\circ$ were carried out.

The results show (see Fig. 15) that the bigger the turbulence intensity in the entrance, the bigger the flow mixing in the inlet zone and the local transition between laminar regime and turbulent regime is less brusque. As expected, turbulence transition may occur for low local Grashof (or Rayleigh) number, if a great turbulence excitation is imposed at inlet. These differences lead to a maximum deviation for Nu_L close to 18% between one case with $I = 2\%$ and other with $I = 20\%$, for the Rayleigh numbers considered in a transitional range ($Ra_L = 10^9$ and $\gamma = \Theta = 0$). For converging channels ($\gamma > 0$), the added graph of Fig. 15 shows that the differences tend to diminish (11% for $\gamma = 6^\circ$ and 3% for $\gamma = 15^\circ$), following the trend pointed above. This is probably due do the relative decrease of

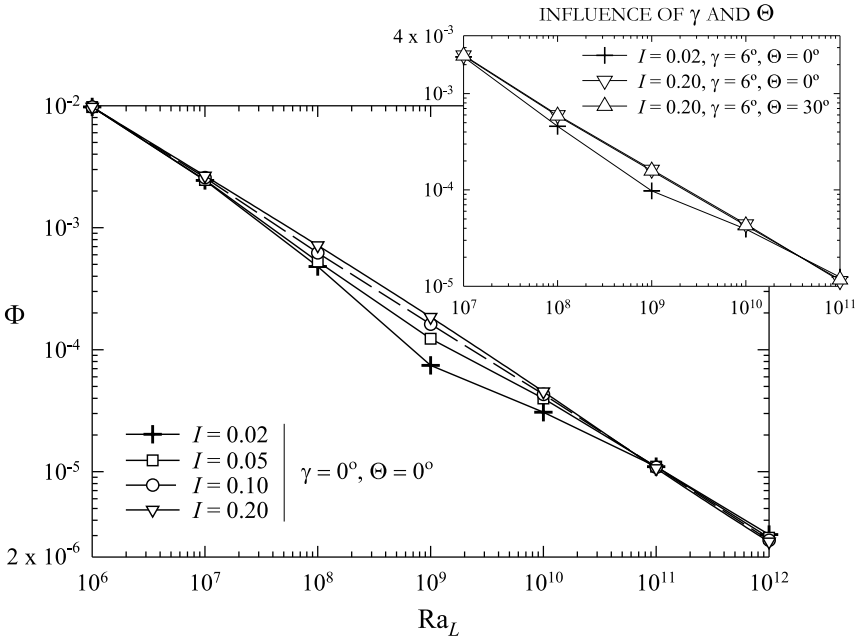

Fig. 16. Non-dimensional mass flow rate Φ as a function of Ra_L. Influence of turbulence intensity I on the transitional range of Ra_L. Isothermal, symmetric heating conditions. $b/L = 0.2$.

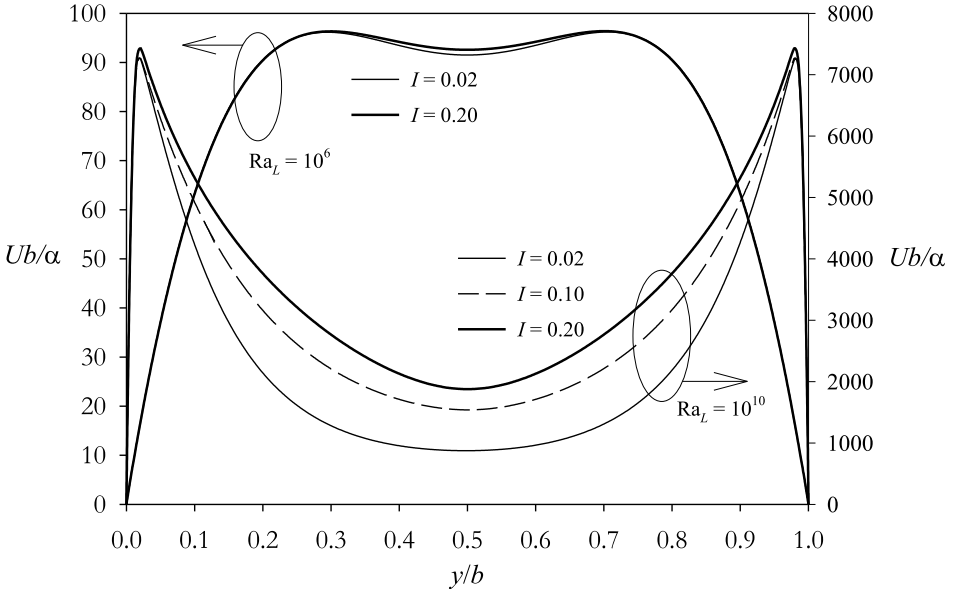

Fig. 17. Profils of mean velocity at outlet of a channel with isothermal, symmetric heating conditions, for two values of Ra_L, 10^6 and 10^{10}, showing the influence of turbulence intensity I. $\gamma = \Theta = 0^\circ$. $b/L = 0.2$.

the velocity at the channel inlet, where the turbulence intensity is imposed. No significant influence of the sloping angle Θ on the effects of I upon Nu_L has been found.

It can be concluded that the differences are really significant in a given range, $Ra_L = 5 \times 10^7 - 5 \times 10^{10}$, within the set of the laminar-turbulent transition. For $Ra_L \geqslant 10^{13}$, deviations reached almost negligible, and results obtained do not show neither in Fig. 15 nor 16.

4.2.4.3. Effects of I on the mass flow behaviour. The effects explained in the last section were much more important on the induced mass flow rate through the channel (Fig. 16). It can be explained by the different influence of turbulence effects over shear and thermal boundary layers, respectively. For Ra_L in the transitional zone, although flow pattern and velocity boundary layer show a similar aspect close to the wall for different values of initial turbulence intensity I, the fluid is compelled to move in the core region in a more significant way for higher values of I (see Fig. 17). This fact drives to obtain a drastic increase in the mass flow rate. These important differences produce also a change in the evolution of Φ as a function of Ra_L for $Ra_L > 10^9$, and, for high enough values of Ra_L, the trend becomes to be identical that those corresponding to strong turbulence flow. For example, for $Ra_L = 10^9$ and $\gamma = \Theta = 0$, deviations with regards to $I = 2\%$ case were equal to 65%, 110% and 150%, for $I = 5\%$, $I = 10\%$, and $I = 20\%$, respectively. While, for $Ra_L = 10^{10}$, deviations were equal to 29%, 40% and 47%, respectively. The differences are lower for fully turbulent flow, as expected. The added graph of Fig. 16 shows that the differences tend to diminish for cases with $\gamma > 0$, following the trend stated above for Nu_L. For example, deviations are equal to 66% and 8% for $\gamma = 6^\circ$ and 15°, respectively, for $Ra_L = 10^9$. Once again, no significant influence of Θ on the effects of I upon Φ has been found.

Finally, the change of trend between asymptotic laminar and fully turbulent behaviour, which clearly can be observed in Fig. 15 for Nu_L, practically do not appears in Fig. 16 for Φ.

5. Concluding remarks

Buoyancy-driven flows in channels for whole range of modified Rayleigh numbers Ra^*, and for different converging and angles (γ) and centreline sloping angles (Θ), have been analyzed. Most of cases were solved for isothermal, symmetric heating conditions. The low-Re k–ω turbulence model was validated through experimental and numerical results taken from literature. The following concluding remarks can be made:

1. The numerical results for turbulent flow linked with the laminar ones obtained in a previous research, Kaiser et al. [20].
2. For turbulent flow, the results obtained showed that aspect ratio b/L influences on non-dimensional mass flow rate Φ in a significant way, probably due to the larger velocity gradients reached, which carry away an appreciable amount of fluid, arising out of the core region. Correlation of the form (29) has been stated.
3. For sloping and convergent channels, the results for Φ could be fitted to those obtained for vertical channels by modification of Rayleigh number through the geometric factor ($\cos\Theta \cos\gamma$).
4. A generalized correlation for Φ has been reported (Eq. (30)), valid for the wide range of Ra^* outlined, involving laminar and turbulent regimes, for a low value of initial turbulence intensity ($I = 2\%$ for the turbulent cases), $0.03 \leqslant b/L \leqslant 0.25$, $0 \leqslant \gamma \leqslant 30^\circ$, and $0 \leqslant \Theta \leqslant 60^\circ$.
5. Finally, effects of initial turbulence intensity I, were much more important on non-dimensional mass flow rate than on average Nusselt number, in the transitional range. High values of I yielded an advance on the transitional Rayleigh number, while low values of I produced a significant deviation from asymptotic behaviour corresponding to strong turbulent flow.

Acknowledgement

This research has been supported by the 'Dirección General de Investigación' of 'Ministerio de Educación y Ciencia' of Spanish Government, through DPI 2003-02719 Project. The computations were carried out in the HPC160 platform of SAIT (Polythecnic University of Cartagena).

References

[1] J.R. Lloyd, E.M. Sparrow, On the instability of natural convection flow on inclined plates, J. Fluid Mech. 42 (1970) 465–470.
[2] M. Miyamoto, Y. Katoh, J. Kurima, Turbulent free convection heat transfer from vertical parallel plates in air (heat transfer characteristics), NACSIS Electron. Libr. Ser. 1 (1983) 1–7.
[3] W.M. Yan, Y.L. Tsay, T.F. Lin, Combined heat and mass transfer in turbulent natural convection between vertical parallel plates, Int. J. Heat Mass Transfer 32 (1989) 1581–1584.
[4] W.M. Yan, T.F. Lin, Heat transfer in buoyancy-driven channel flows with the simultaneous presence of laminar, transitional and turbulent flow regimes, Warme-und Stoffubertragung 24 (1989) 125–132.
[5] W.M. Yan, T.F. Lin, Theoretical and experimental study of natural convection pipe flows at high Rayleigh number, Int. J. Heat Mass Transfer 34 (1991) 291–303.
[6] X. Yuan, A. Moser, P. Suter, Wall functions for numerical simulation of turbulent natural convection along vertical plates, Int. J. Heat Mass Transfer 36 (1993) 4477–4485.
[7] T.A. Versteegh, F.T. Nieuwstadt, A direct numerical simulation of natural convection between two infinite vertical differentially heated walls scaling laws and wall functions, Int. J. Heat Mass Transfer 42 (1999) 3673–3693.
[8] R.A.W.M. Henkes, C.J. Hoogendorn, Comparison exercise for computations of turbulent natural convection in enclosures, Numer. Heat Transfer 28 (1995) 59–78.
[9] S. Peng, L. Davison, Computation of turbulent buoyant flows in enclosures with low-Reynolds number k–ω models, Int. J. Heat Fluid Flow 20 (1999) 172–184.
[10] W. Xu, Q. Chen, F.T.M. Nieuwstadt, A new turbulence model for near wall natural convection, Int. J. Heat Mass Transfer 41 (1998) 3161–3176.

[11] S.A.M. Said, M.A. Habib, H.M. Badr, S. Anwar, Turbulent natural convection between inclined isothermal plates, Comput. Fluids 34 (2005) 1025–1039.
[12] A.G. Fedorov, R. Viskanta, Turbulent natural convection heat transfer in an asymmetrically heated, vertical parallel-plate channel, Int. J. Heat Mass Transfer 40 (1997) 3849–3860.
[13] M. Miyamoto, Y. Katoh, J. Kurima, H. Suki, Turbulent free convection heat transfer from vertical parallel plates, in: C.L. Tien, V.P. Carey, J.K. Ferrel (Eds.), Heat Transfer, vol. 4, Hemisphere, Washington, DC, 1986, pp. 1593–1598.
[14] A. Hajji, W.M. Worek, Analysis of combined fully developed natural convection heat and mass transfer between two inclined parallel plates, Int. J. Heat Mass Transfer 31 (1988) 1933–1940.
[15] K.T. Lee, Natural convection in vertical parallel plates with an unheated entry or an unheated exit, Numer. Heat Transfer 25 (1994) 477–493.
[16] W. Aung, Fully developed laminar free convection between vertical plates heated asymmetrically, Int. J. Heat Mass Transfer 15 (1972) 1577–1580.
[17] D.J. Nelson, B.D. Wood, Fully developed combined heat and mass transfer natural convection between parallel vertical plates with asymmetric boundary conditions, Int. J. Heat Mass Transfer 32 (1989) 1789–1792.
[18] Z.Y. Guo, X.B. Wu, Thermal drag and critical heat flux for natural convection of air in vertical parallel plates, ASME J. Heat Transfer 115 (1993) 124–129.
[19] J. Hernández, B. Zamora, Effects of variable properties and non-uniform heating on natural convection flows in vertical channels, Int. J. Heat Mass Transfer 48 (2005) 793–807.
[20] A.S. Kaiser, B. Zamora, A. Viedma, Correlation for nusselt number in natural convection in vertical convergent channels at uniform wall temperature by a numerical investigation, Int. J. Heat Fluid Flow 25 (2004) 671–682.
[21] D.C. Wilcox, Turbulence Modeling for CFD, second ed., DCW Industries, USA, 2003.
[22] A.N. Kolmogorov, Equations of turbulent motion of an incompresible fluid, Izvestia Acad. Sci. USSR, Phys. 6 (1942) 56–58.
[23] J. Hernández, B. Zamora, A. Campo, On the effect of Prandtl number and aspect ratio upon laminar natural-convection flows in vertical channels, in: Proc. Tenth International Heat Transfer Conference, vol. 5, 1994, pp. 483–488.
[24] S.V. Patankar, D.B. Spalding, A calculation procedure for heat, mass and momentum transfer in three-dimensional parabolic flows, Int. J. Heat Mass Transfer 15 (1972) 1787–1806.
[25] B. Van Leer, Towards the ultimate conservative difference scheme V. A second order sequel to Gadunov's method, J. Comput. Phys. 32 (1979) 101–136.
[26] S.W. Churchill, J.F. Usagi, A general expression for the correlation of rates of transfer and other phenomena, AIchE J. 18 (1972) 1121–1128.
[27] H. Akbari, T.R. Borgers, Free convective turbulent flows within the Trombe Wall channel, Solar Energy 33 (1984) 253–264.
[28] T. Chen, Laminar and Turbulent Natural Convection Heat Transfer in Trombe Wall Channels. Ph.D. Thesis, Old Dominion University, 1992.
[29] M.A. Habib, S.A.M. Said, S.A. Ahmed, A. Asghar, Velocity characteristics of turbulent natural convection in symmetrically and asymmetrically heated vertical channels, Exp. Therm. Fluid Sci. 26 (2002) 77–87.
[30] S.W. Churchill, H.H.S. Chu, Correlating equations for laminar and turbulent free convection from a vertical plate, Int. J. Heat Mass Transfer 18 (1975) 1323.